Geomechanics and Engineering, *Vol. 43, No. 4 (2025) 259-267*
https://doi.org/10.12989/gae.2025.43.4.259

Influence of leakage under different joint locations on river-crossing tunnels: Experimental and numerical investigation

Yu Xiang[1], Bai Shuaiqiang[1], Chen Can[2], Wang Yuke*[1] and Xue Yujie[3]

[1]*School of Water Conservancy and Transportation, Zhengzhou University, Zhengzhou, China*
[2]*Henan Hydrology and Water Resources Center, Zhengzhou, China*
[3]*College of Vehicle and Traffic Engineering, Zhengzhou University of Science and Technology, Zhengzhou, China*

(*Received July 11, 2023, Revised October 22, 2025, Accepted October 24, 2025*)

Abstract. Joint leakage is one of the major defects in river-crossing tunnels during operation period. The influence of leakage under different joint locations on the tunnel structure is different. In this paper, a combination of model tests and numerical simulations was developed to investigate the influence of leakage under different joint locations during operation period on the tunnel structure and the strata. Specifically, the difference of joint permeability coefficients with different locations was considered, and the formula quantifying the relationship between the permeability coefficient and the angle of joint was established. Nanjing Dinghuaimen River-Crossing Tunnel in China was used as the engineering background to study the leakage patterns for different locations of joints. The results show that the tunnel structure responds more to leakage at tunnel arch bottom and foot during operation period. When leakage occurs at tunnel arch foot, the infiltration volume is 33.6% more than that at the tunnel vault, and the surface settlements are 2.4 times more than that at the tunnel vault. The surface settlement caused by the joints is related to the infiltration volume. The location of the joints affects the shape of the lining deformation and the overall deformation is less. The results of this paper have certain guiding significance for tunnel maintenance projects.

Keywords: joint leakage location; model test; operation period; river-crossing tunnel

1. Introduction

Shield tunnels are increasingly being used in cross river and sea passage projects due to their advantages of low construction disturbance and high engineering quality (Zhang *et al.* 2017, Zhang *et al*. 2023). The tunnel safety problems are increasingly exposed with the increase of tunnel engineering scale and operation time (Kim *et al.* 2020). Due to the multi-joint structure of shield tunnels, leakage problems are the most common type of safety problems in shield tunnels. According to statistics, tunnel leakage safety problems are concentrated in "holes" and "joints", among which joint leakage is the main form of leakage (Wei and Lin 2013). In the high-water pressure environment under the river, a greater risk of leakage is assumed in shield tunnelling due to the presence of a large number of joints (Zhang *et al.* 2021). The influence of leakage under different joint locations on the tunnel structure is different. Therefore, analyzing the influence of leakage under different joint locations on river-crossing tunnels during operational period is indispensable.

In recent years, the influence of tunnel leakage has been thoroughly studied by scholars. The assumption of uniform leakage in tunnels is adopted by early researchers (Ming *et al.* 2010, Park *et al.* 2008, Wang and Li 2018). It has been found that the greater the permeability of the lining relative to the soil, the more severe the influence of leakage (Gong *et al.* 2022, Kolymbas and Wagner 2007, Shin *et al.* 2002). Zhang *et al.* (2026) simulated the leakage of longitudinal joints at different positions based on the assumption of plane strain, and pointed out the significant difference between joint leakage and uniform leakage.

Common methodologies for investigating tunnel joint leakage include theoretical analysis, physical modeling test, and numerical simulation. In the existing research on tunnel joint leakage, the theoretical analysis method has been supplemented and improved by scholars, becoming increasingly close to actual working conditions. The water blocking effect of lining (Fahimifar and Zareifard 2013), leakage conditions (Arjnoi *et al.* 2009, Lei 1999), stress relaxation of lining (Kabwe *et al.* 2020), soil and water pressure loads on lining (Liu *et al.* 2021), anisotropic soils (Tang *et al.* 2018) have been considered by scholars. Additionally, the model test has been adopted by most scholars for tunnel leakage testing. Through model tests, Zhang *et al.* (2013) studied the effect of tunnel leakage on tunnel settlement and lining moment, considering both finite permeable and impermeable lining inflow regimes. Lu *et al.* (2019) experimentally investigated the leakage process in shield tunnels under constant water pressure, testing the effects of assembly patterns, leak widths, and locations. Gao *et al.* (2019) carried out a model test study of tunnel lining leakage safety problems under different burial depth conditions. With the development of computer technology, various numerical simulation methods have been used to make research closer to actual operating conditions. Whereas Hassani *et al*. (2016) prioritized model

*Corresponding author, Professor
E-mail: ykewang@163.com

ISSN: 2005-307X (Print), 2092-6219 (Online)

dimensions in predicting groundwater inflow, and Wongsaroj *et al.* (2007) incorporated soil anisotropy in studying leakage response, subsequent research has refined the numerical modeling of leakage effects. Gong *et al.* (2022) parametrically analyzed impacts on lining and settlement, while Wu *et al*. (2020) and Wang *et al.* (2020) proposed advanced numerical and analytical methods, respectively. In contrast, the joint coefficient is inversely inferred based on the leakage limit during tunnel design. The joint permeability coefficient obtained varies depending on the working conditions studied by scholars (Zhang *et al*. 2013).

Despite these significant advances, several key limitations remain to be addressed. The vast majority of current theoretical analysis is two-dimensional, with numerous hypotheses based on semi-infinite or infinite planes. In physical modeling tests, scholars have not conducted satisfactory research on complex situations such as three-dimensional local leakage. The conditions of model tests are increasingly close to actual operating conditions, but fewer studies on the influence of leakage under different joint locations during operational period. The permeability coefficient of the joint obtained by traditional method is only related to the number of joints, the difference of joint permeability coefficients with different locations was not considered, which is not in line with actual engineering.

To address these limitations, this study investigates the effects of leakage under different joint locations on the tunnel structure and the strata during operation, using physical modeling and numerical analysis. The study is based on the assumptions of soil homogeneity and simplified bolt-joint interactions. Firstly, a self-design model test was established to study the leakage patterns of leakage under different joint locations. Secondly, the formula quantifying the relationship between the permeability coefficient and the angle of joint was established based on the theory of fracture seepage. Finally, the numerical model was established based on a typical cross-section of the Dinghuaimen Tunnel. The variations of displacement and seepage fields due to leakage under different joint locations were analyzed in the numerical model. Joint location is identified as a key variable. This finding is essential for developing more accurate theoretical models of tunnel seepage. The findings provide a crucial theoretical basis for tunnel safety throughout their lifecycle, thereby enhancing the long-term safety and economic viability of such projects.

2. Leakage of joints model test

In the Nanjing Dinghuaimen river-crossing Tunnel, a typical cross-sectional tunnel with high-water pressure and thin soil covered was selected as the research object. A visual testing device for the river-crossing tunnel leakage that can control locations of joints was designed to conduct a model test. On the tunnel model, 5 tunnel joints of 1mm width with different locations were set to leakage, namely the tunnel vault 0°, tunnel spandrel 45°, tunnel arch waist 90°, tunnel arch foot 135°, and tunnel arch bottom 180°.

Fig. 1 Introduction of the Dinghuaimen Tunnel Project

The leakage conditions of individual joint leakage were set to investigate the joint leakage patterns.

2.1 Engineering background

The Dinghuaimen Tunnel is a river-crossing shield tunnel spanning the Yangtze River in Nanjing, Jiangsu Province, China. As shown in Fig. 1, it consists of a southern line and a northern line. The total length of the northern line is 7014 m, with the underwater part of 4135 m. The total length of the southern line is 7363 m, with the underwater part of 3557 m. The underwater geological conditions of the Dinghuaimen Tunnel project are complex, with a maximum soil cover thickness of about 51 m. The maximum water depth above the arch of the middle section of the river-crossing tunnel is about 62.3 m, and the maximum water pressure at the river-crossing section of tunnel is about 0.76 MPa. Compared with other tunnels of the same type, the Dinghuaimen Tunnel is the largest, longest, most geologically complex, and highest water pressure tunnel. This tunnel has been given special attention and has great research value for leakage problems at tunnel joints. In this paper, to study the influence of leakage under different joint locations, a typical section of the tunnel project with high water pressure and thin soil coverage as the research object was selected.

2.2 Model test

2.2.1 Test equipment

The geometric similarity ratio of this experiment is C_l =100. A tunnel test equipment with controlled leakage point location was designed. The equipment consists of a test chamber, a model river-crossing tunnel, a water and sand collection system, and a data collection system.

As shown in Fig. 2, the main test chamber is made of 3 mm thick steel plate, and the size of the main skeleton is 1500 mm × 1000 mm × 600 mm. The length is set to 1500 mm to ensure a minimum distance of 5.6D from the boundary on both sides to the tunnel centerline. The front of the steel plate is hollowed out around the tunnel and its surrounding areas, and a 20 mm transparent acrylic is plated onto the inside walls of the test chamber to form a visual window. In order to further reduce the influence of bottom boundary effect, the distance between the bottom of the simulated tunnel hole and the bottom of the test chamber is set to 260 mm. The edge of the test chamber is sealed with silicone coating for waterproofing.

As shown in Figs. 3-5, the model tunnel is made of stainless-steel material. The model tunnel dimensions are 146 mm (outer diameter) × 600 mm (length), with a 6-mm wall

Fig. 2 Main test chamber

Fig. 3 Model of river-crossing tunnel

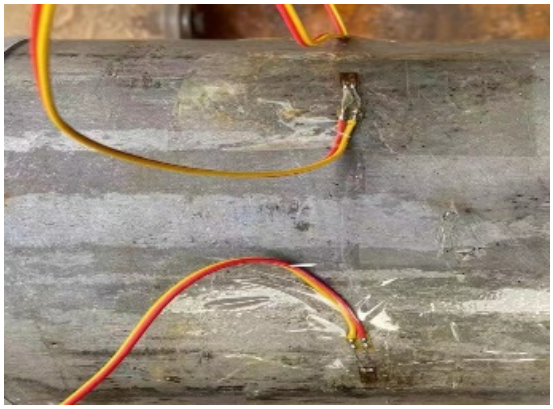

Fig. 4 Pasting of strain gauge outside the tunnel

Fig. 5 Pasting of strain gauge inside the tunnel

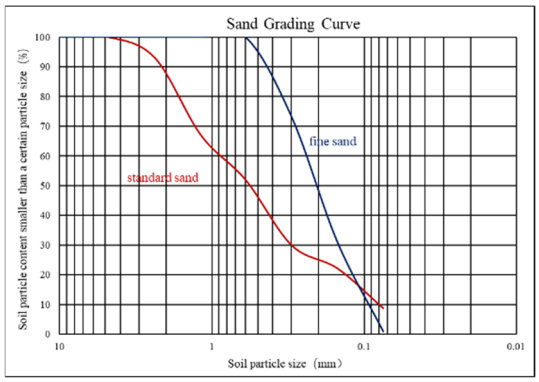

Fig. 6 Test find sand grading curve

thickness. At the same section of the model tunnel, 1 mm × 10 mm joints at different locations are set. The segments near the leakage of tunnel joints are pasted with resistance strain gauge, which are respectively located at the Tunnel vault, Tunnel spandrel, Tunnel arch waist and Tunnel arch foot. Bridge type earth pressure sensors are arranged on the outer side of the tunnel joint and connected to the data acquisition system. The model tunnel is placed at the preset opening of the model chamber, and the gaps in contact are sealed with transparent glass adhesive. The water and sand collection system of the experimental device consists of a single inclined drainage tube and a series of measuring cylinders. The outer diameter of the monoclinic drainage tube is set to be consistent with the inner diameter of the tunnel. In order to reduce disturbance near the leakage of tunnel joint, a plastic film with a certain slope is laid in the model tunnel to guide the water and sand quickly flow out into the measuring cylinder.

2.2.2 The sample of test soil

According to the engineering geological survey report, the main stratum crossed by the project in the middle section of the Yangtze River is fine sand. Fine sand was used as the soil sample of this model test. The grading curve of this fine sand is shown in Fig. 6. Although the fine sand is poorly graded compared to the standard sand, it can reflect the actual underwater working conditions of the Dinghuaimen Tunnel.

The Mohr-Coulomb constitutive model was adopted in this model test, the dry density ρ is 1.91 g/cm^3. The void ratio e is 0.73. The angle of internal friction φ is 34.1°. The elastic modulus E is 400 kPa. The Poisson ratio μ is 0.29. The permeability coefficient k is 8.21×10^{-6} m/s. In the model test, the density similarity ratio is α_ρ=1. The Poisson's ratio similarity ratio is α_μ=1. The similarity ratios are α_e=1 for void ratio, α_φ=1 for internal friction angle, α_E=100 for elastic modulus, and α_k=1 for permeability coefficient.

Although the experimental soil samples used in this paper are poorly graded, the simulation of leakage of the river-crossing tunnel joints can be achieved. Accurate leakage data of 1 mm tunnel joints can be obtained through experiments to explore the leakage patterns of different joint locations.

A leakage model test is conducted at the tunnel joint with a width of 1 mm based on the above experimental equipment and materials. The distribution of each joint is shown in Fig. 7, with five different locations of joint, namely at 0 ° of the tunnel

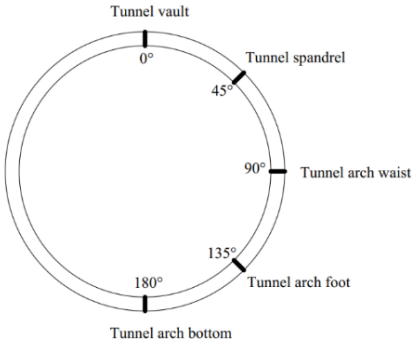

Fig. 7 Schematic diagram of leakage distribution at differ ent joint locations

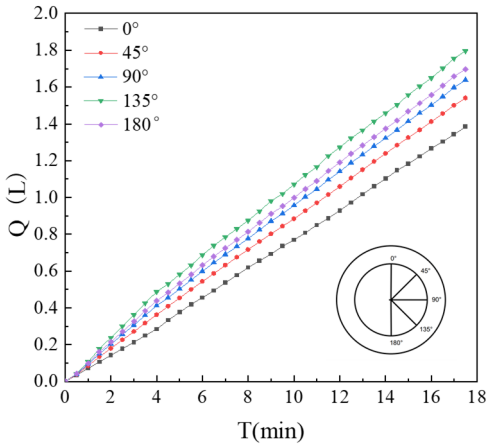

Fig. 8 The infiltration volume of leakage under different joint locations

vault, 45 ° of the tunnel spandrel, 90 ° of the tunnel arch waist, 135 ° of the tunnel arch foot, and 180 ° of the tunnel arch bottom. The duration of each test is set to 15 h, and a single joint leakage is set for each test. 160 mm is set as the thickness of the soil cover above the arch, and the water level line is located 410 mm above the surface of the tunnel soil.

2.3 Test procedure

(1) A certain amount of fine sand was poured into a test chamber of the same height using the falling rain method. The layered compaction method was used to prepare fine sand layers of specified density. During the sand filling process, each layer of fine sand was laid flush with the scale lines (spaced 100 mm apart) on the test chamber at the initial moment. Each layer surface was manually compacted by 25 blows with a 10-kg hammer dropping from a height of 30 cm to ensure that each layer achieved the target compaction level. In each working condition, the fine sand layer was finally filled to a height of approximately 566 mm from the bottom of the test chamber, which means that the soil cover thickness C of the model tunnel is 160 mm ($C/D \approx 1.1 < 2.0$, belonging to a shallow buried tunnel) (Qiu *et al.* 2019).

(2) Water was slowly injected from one side of the test chamber to a height of 976 mm from the bottom of the test chamber, which is 410 mm above the model tunnel. Allow to stand for 24 h until the fine sand was fully consolidated. After the leakage test started, water was slowly injected into the model chamber to maintain the water level unchanged.

(3) The monoclinic drainage tube was placed into the model tunnel, and the waterproof tape at the joint was gently pulled out to make it start to leak water and sand. After the experiment begins, water and sand naturally flow out from the opening on the front of the test chamber into the measuring box directly below the tunnel outlet. The measuring box for collecting water and sand leaks was replaced every 30 seconds and the number of the measuring boxes was recorded (Zhang *et al.* 2026). When the sand leakage converges (only water leakage), data was recorded every 2 minutes, and at least 6 sets of box numbers for collecting water leakage were collected.

(4) After extracting the waterproof tape, the readings of the soil pressure gauge data collection system were extracted every 2 minutes.

(5) Residual water and sand in the test chamber were cleaned up. The wet sand flat was laid on a plastic film to dry. Check if the instrument was connected properly. The leakage test at the same joint locations was repeated as a control test to take the average of the two test results for analysis.

2.4 Test results and discussion

Fig. 8 shows the leakage rate of joints in different parts of the tunnel over time. It can be seen that the infiltration volume of joint steadily increases with the increase of leakage time T. The rate leakage of tunnel joint is basically not affected by time T. The infiltration volume and seepage rate vary greatly in different joint locations of the tunnel, with the maximum seepage flow rate appearing at the tunnel arch foot. It is observed that the seepage volume is highest at the tunnel arch foot, followed by the tunnel arch bottom, tunnel arch waist, tunnel spandrel, and tunnel vault. The infiltration volume is positively proportional to the burial depth of the tunnel. However, due to the need for water to overcome gravity during leakage at the tunnel arch bottom, the infiltration volume at the tunnel arch bottom is smaller than that at the tunnel arch foot. During the same time period, the leakage of tunnel joint at the tunnel arch foot is 33.6% higher than that at the tunnel vault, so it should be given more attention when there is leakage at the tunnel arch foot.

3. Numerical simulation of joint leakage

There is a size effect in the model test, and the results are primarily used for mechanism analysis and pattern analysis. The results are detected by the arrangement of sensors, so it is not possible to conduct comprehensive and systematic detection of seepage and stress fields. The long-term joint leakage test of tunnels is also limited by objective conditions such as time and cost. The finite element method is used to establish numerical models for leakage of tunnel joints in different locations can obtain more accurate stress and seepage field data, and the limitations of model testing conditions is compensated.

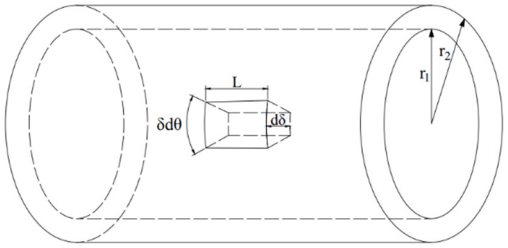

Fig. 9 Joint model with a length of L

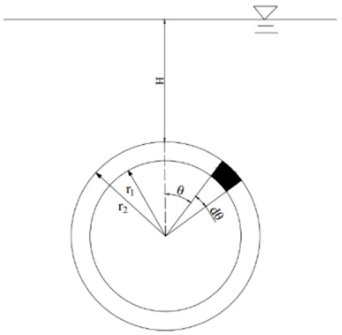

Fig. 10 Joint model with a water level of H

Firstly, based on the theory of fracture seepage, the formula quantifying the relationship between the permeability coefficient and the angle of joint was derived. Then, based on the measured infiltration volume through model tests, the permeability coefficients of different joints locations were calculated. Finally, based on the finite element software and the basic work done earlier, a numerical calculation model was established. This method makes the established numerical model closer to the actual working conditions. The influence of leakage at different joint locations on stress and seepage fields can be studied more comprehensively by numerical model.

3.1 Confirmation of joint permeability coefficient

The theoretical analysis method and model test method have limitations in practical engineering applications, and numerical simulation method has become a popular method for studying tunnel leakage problems.

The permeability coefficient of joint is confirmed with a single method at present. The permeability coefficient obtained through this method is changed based on the number of joints set. However, in actual working conditions, leakage of tunnel lining at different joint locations have different seepage forces due to different external water pressures. According to the conclusions of the model tests, it can be concluded that the infiltration volume varies at different joint locations. Therefore, the permeability coefficient of tunnel joints varies from different locations.

A leakage model of the single tunnel joint is shown in Figs. 9-11. The lining effect is considered. The soil is simplified into a semi-infinite body. The soil, tunnel, and lining are considered isotropic media. The inner radius of the lining is determined as r_1, the outer radius of the tunnel lining is determined as r_2, and the water level is determined as H. The joint model with a length of L is shown in Fig. 9, and the model has the following assumptions (Kolymbas and Wagner 2007):

(1) The permeability of the lining segment is assumed to be 0.

(2) The water level is assumed to remain constant at a height of H.

(3) the interface between the inner side of the soil and the outer side of the lining is assumed a constant head boundary. The inner surface of the tunnel is assumed under normal pressure, with a water head height of 0.

(4) Any dθ Within the angle, the tunnel lining bears uniform longitudinal stress, and the main variables in different calculation micro ends are named J_f and δ.

(5) The leakage of the lining joint only follows the normal direction is assumed, so the flow rate q_{ij} is considered equal for leakage of any angle range dθ

According to hypothesis (1), the permeability coefficient of stable joint can be obtained from the square law of crack seepage (Yan and Zheng 2017)

$$k_{\mathrm{f}} = \frac{gL^2}{12\eta} \tag{1}$$

η------ the viscosity coefficient of water.

As shown in Formula (2), the hydraulic gradient within each microsection is expressed as the pressure difference between the inner and outer sides of the microsection and the length ratio.

$$J_{\mathrm{f}} = \frac{\mathrm{d}h_{\mathrm{w}}}{\mathrm{d}\delta} \tag{2}$$

At any circumferential seam width δ_jdθ of Within the micro segment, the flow q_{ij} is expressed by Formula (3) which can be introduced by the association of Formulas (1)and (2).

$$q_{ij} = \frac{gL^3 \mathrm{d}h_{\mathrm{w}_{ij}}}{12\eta \mathrm{d}\delta_j}\delta_{ij}\mathrm{d}\theta \tag{3}$$

According to the assumption, at any dθ Within the range, the infiltration rate through different micro elements along the normal direction is equal. Represented as: q_{i1}= q_{i2}= q_{i3}=...= q_{in}. It is shown in Formula (4).

$$q_{i1} = \frac{gL^3 \mathrm{d}h_{\mathrm{w}_{i1}}}{12\eta \mathrm{d}\delta_{i1}}\delta_{i1} = \frac{gL^3 \mathrm{d}h_{\mathrm{w}_{i2}}}{12\eta \mathrm{d}\delta_{i2}}\delta_{i2} = \cdots = \frac{gL^3 \mathrm{d}h_{\mathrm{w}_{in}}}{12\eta \mathrm{d}\delta_{in}}\delta_{in} \tag{4}$$

According to the assumption, the water head at a certain point outside the lining ring is shown in Formula (5).

$$p = \rho_w g\left[\mathrm{H}+r_2\left(1-\cos\theta\right)\right] \tag{5}$$

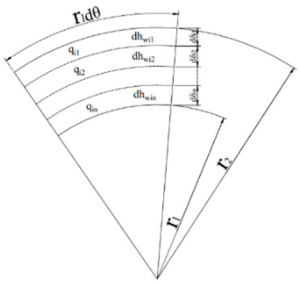

Fig. 11 Joint model with inner and outer radius

Table 1 Permeability coefficient of 1 mm joint

Angle	0°	45°	90°	135°	180°
K_f(m/s)×10^{-4}	3.42	3.8	4.05	4.45	4.21

The traffic of within the micro element q_i for any angle dθ is obtained though integrate along the normal direction ($r_1 \rightarrow r_2$), as shown in Formula (6) which can be introduced by the association of Formulas (3), (4) and (5).

$$q_i = \frac{g^2 L^3 \rho_w \left[\mathrm{H}+r_2\left(1-\cos\theta\right)\right]\left(r_2-r_1\right)}{12\eta \ln\left(r_2/r_1\right)} r_i \mathrm{d}\theta \qquad (6)$$

Therefore, in the case of any $\theta_1 \rightarrow \theta_2$, the total seepage flow rate of the tunnel at the through lining joint of length L is represented Formula (7).

$$\mathrm{Q}=\frac{k_f L \rho_w g\left(r_2-r_1\right)}{\ln\left(r_2/r_1\right)}\left[\left(\mathrm{H}+r_2\right)\left(\theta_2-\theta_1\right)+r_2\left(\sin\theta_2-\sin\theta_1\right)\right] \qquad (7)$$

3.2 Model establishment

A "lining-soil" tunnel joint leakage calculation model was established based on the finite element software ABAQUS. The working conditions of the finite element model and the model test were the same. The section of the Dinghuaimen Tunnel with the deepest river water and the thinnest soil covering the tunnel was selected. In numerical models, the soil size was 150 m × 70 m. The outer diameter of the tunnel lining was 14.5 m. The thickness of the tunnel lining was 0.6 m and the thickness of the soil layer above the tunnel was 16 m. The water level above the tunnel was set as 57 m.

The Mohr-Coulomb constitutive model was adopted by the numerical model of soil. The dry density ρ of the fine sand was 1.91 g/cm^3. The void ratio e was 0.73. The angle of internal friction φ was set to 34.1°. The Cohesive force c was 9 kPa. The Elastic Modulus E was 39.6 MPa. The Poisson ratio μ was 0.29. The permeability coefficient k was 8.23×10^{-6} m/s.

C60 concrete was used as the lining of the shield tunnel. A linear-elastic constitutive modeling is used to simulate its mechanical behavior. The bolt connection between tunnel lining segments was not considered, the equivalent stiffness

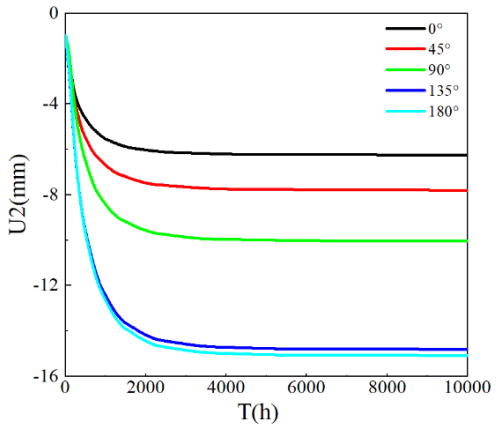

Fig. 12 Surface settlement above the tunnel vault over time

method was used to simplify the tunnel into a homogeneous concrete ring (Gong *et al*. 2022). The elastic modulus E of the tunnel lining segment was 24 GPa. The lining weight was taken as 24 kN/m^3. The permeability coefficient of the lining is 10^{-13} m/s according to the design standards. The permeability coefficient of 1 mm joints at different locations in the model tests were calculated according to Formular (7), as shown in Table 1. The CPE4P fluid solid coupling calculation element was selected for both the tunnel soil and lining elements.

The model is mainly divided into three calculation and analysis steps: Crustal stress balance analysis step. The initial crustal stress distribution of the tunnel under self-weight after excavation was simulated; Load analysis steps. A pressure identical to the water pressure of the model test is applied to the soil; Analysis steps for seepage consolidation. The inner boundary pore water pressure of the tunnel lining was set to 0. The leakage duration is 10000h.

4. Result analysis

4.1 Analysis of the influence of leakage under different joint locations on surface settlement and tunnel deformation

As shown in Fig. 12, the surface settlement above the tunnel vault is altered by time. It can be seen that 10000 h can fully simulate the entire process of the tunnel from joint leakage to stable state. From the data in Fig. 12, It can be seen that when leakage occurs at tunnel arch bottom, the maximum amount of surface settlement is 15.08 mm. The surface settlement amount when there is leakage at the tunnel arch foot is not significantly different from the tunnel arch bottom, which is 14.81 mm. Special attention should be paid when there is leakage at the tunnel arch bottom and the tunnel arch foot.

The surface settlement is shown in Fig. 13. The soil surface settlement above the tunnel is affected by joint leakage. The surface settlement pattern is influenced by the locations of the joint. Surface settlement decreases as the distance from the tunnel increases. As the tunnel leakage location is deeper, the surface settlement is larger. Surface settlement was influenced

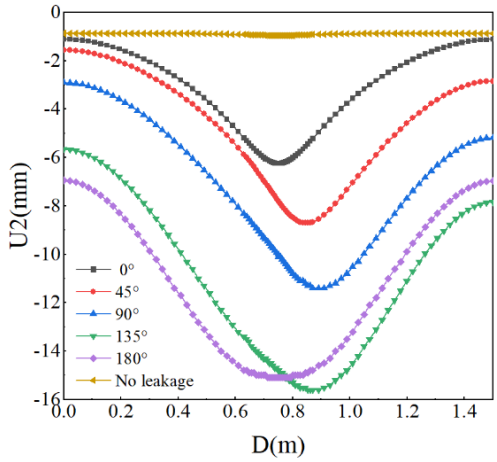

Fig. 13 Analysis of surface settlement due to leakage at d ifferent joint locations

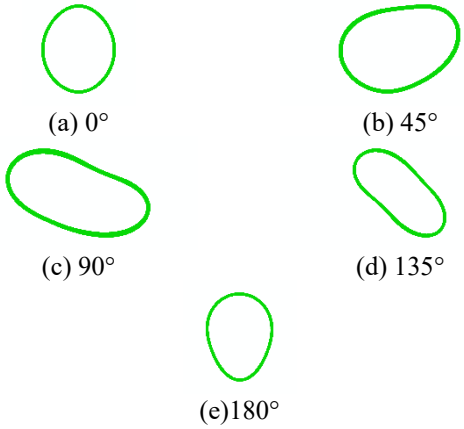

Fig. 14 Deformation diagram of leakage lining at different joint locations

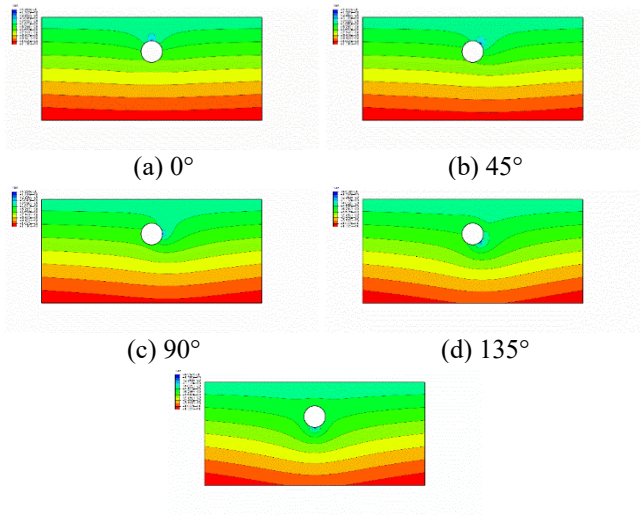

Fig. 15 Distribution of lining pore water pressure for leakage at different joint locations

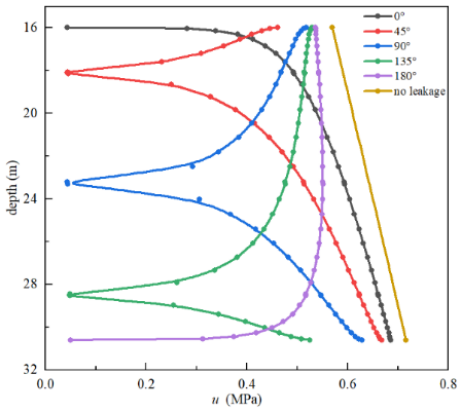

Fig. 16 Pore water pressure and burial depth at leakage of tunnel joints

minimally by leakage of the tunnel vault. The maximum settlement is 6.24 mm. The surface settlement is most influenced by the foot of the tunnel arch. The surface settlement caused by leakage at the tunnel foot was 2.4 times more than that at the tunnel vault.

The deformation diagram of leakage under different joint locations is shown in Fig. 14. The deformation coefficient of the lining is magnified by 500 times in Fig. 14. The location of the joints affects the shape of the lining deformation and the overall deformation is less. When leakage occurs at the tunnel vault and tunnel arch bottom, the tunnel lining deforms into a vertical ellipse. When leakage occurs in the tunnel spandrel, tunnel arch waist, and tunnel arch foot, the tunnel lining deforms into a transverse ellipse. The most common occurrence of joint opening is at the tunnel arch waist, and special attention should be paid when leakage occurs in the tunnel. Special attention should be paid when leakage occurs in the tunnel.

4.2 Analysis of leakage pattern of different joint locations

Distribution of lining pore water pressure for leakage at different joint locations is shown in Fig. 15. The pore water pressure near the leakage site decreases. The distribution of pore water pressure in the soil far away from the leakage site is also affected. The relationship between pore water pressure and burial depth at the leakage site under different conditions is shown in Fig. 16. When leakage occurs at the tunnel vault, tunnel spandrel, arch waist, arch foot, and arch bottom, the pore water pressure value of the soil layer near the leakage of tunnel joint is: 0.0449 MPa, 0.0440 MPa, 0.0450 MPa, 0.0451 MPa, and 0.0498 MPa, respectively. The pore water pressure of the arch bottom joint leakage is smaller than that of other parts. The closer the joint is to the arch bottom, the more significant the decrease in pore water pressure around the tunnel and the influence is greater. The influence of leakage at different joints on the distribution of pore water pressure is most pronounced at tunnel arch bottom, followed by tunnel arch foot, tunnel arch waist, tunnel spandrel, and tunnel vault. When leakage occurs, the pore water pressure of the soil layer next to the leakage of tunnel joint decreases by 90.83%, 91.22%, 92.99%, 93.51%, 93.05%. The influence on pore water pressure is most pronounced at the tunnel arch foot, followed by tunnel arch bottom, tunnel arch waist, tunnel spandrel, and tunnel vault.

5. Conclusions

In this paper, a series of experiments and numerical analyses were carried out to study the influence of 1 mm joint leakage at different locations on the tunnel and strata. The leakage pattern was preliminarily studied based on the infiltration volume. The formula for the joint permeability coefficient influenced of different angles was derived based on the theory of fracture seepage. The variations of displacement and seepage fields due to leakage in different joints locations were analyzed in the numerical model. The main conclusions of this paper are as follows:

• The tunnel structure responds more to leakage at tunnel arch bottom and foot during operation period. When leakage occurs at tunnel arch foot, the infiltration volume is 33.6% more than that at the tunnel vault, and the surface settlements are 2.4 times more than that at the tunnel vault. The surface settlement caused by the joints is related to the infiltration volume. The seepage volume is highest at the tunnel arch foot, followed by the tunnel arch bottom, tunnel arch waist, tunnel spandrel, and tunnel vault. The infiltration volume at the tunnel arch bottom is smaller than the infiltration volume at the tunnel arch foot due to the influence of gravity.

• The permeability coefficients of 1 mm joints at the tunnel vault, tunnel spandrel, tunnel arch waist, tunnel arch foot, and tunnel arch bottom are 3.42×10^{-4} m/s, 3.81×10^{-4} m/s, 4.05×10^{-4} m/s, 4.45×10^{-4} m/s, 4.21×10^{-4} m/s, respectively.

• The location of the joints affects the shape of the lining deformation and the overall deformation is less. When leakage occurs at the tunnel vault and tunnel arch bottom, the tunnel lining deforms into a vertical ellipse. When leakage occurs in the tunnel spandrel, tunnel arch waist, and tunnel arch foot, the tunnel lining deforms into a transverse ellipse.

• The closer the leakage of tunnel joint to the tunnel arch bottom, the more significant the decrease in pore water pressure around the tunnel joint. The pore water pressure near the tunnel arch bottom joint is greater than that at the tunnel arch foot based on the numerical simulation. The decrease of pore water pressure near the tunnel arch foot joint is greater than the tunnel arch bottom.

By advancing the understanding of seepage from occurrence to its spatial variation, this study highlights joint location as a critical variable for accurate seepage modeling. This provides a theoretical foundation for improving tunnel safety and economic viability throughout the project lifecycle. This study is subject to limitations, primarily its reliance on core simplifying assumptions such as the use of isotropic fine sand and the simplified treatment of bolt-joint interactions. It employs homogeneous, poorly graded sand to create a repeatable model at the expense of simulating in-situ heterogeneity. Therefore, investigating the long-term steady-state behavior of tunnels, incorporating soil anisotropy, heterogeneity, and complex interface behavior, is a critical research direction. This will be addressed in future work through longer-duration physical model tests or advanced numerical simulations.

Acknowledgments

The work present in this paper was supported by Excellent Youth Fund of Henan Natural Science Foundation (232300421069); Central Plains Science and Technology Innovation Leader Project (234200510014). These financial supports are gratefully acknowledged.

References

Arjnoi, P., Jeong, J.H., Kim, C.Y. and Park, K.H. (2009), "Effect of drainage conditions on porewater pressure distributions and lining stresses in drained tunnels", *Tunn. Undergr. Sp. Tech.*, **24**(4), 376-389. https://doi.org/10.1016/j.tust.2008.10.006.

Fahimifar, A. and Zareifard, M.R. (2013), "A new closed-form solution for analysis of unlined pressure tunnels under seepage forces", *Int. J. Numer. Anal. Method. Geomech.*, **37**(11), 1591-1613. https://doi.org/10.1002/nag.2101.

Gao, C., Li, S., Lin, C., Li, L., Zhou, Z., Liu, C. and Sun, S. (2019), "Development and application of model test system for water leakage disease in tunnel lining", *Rock Soil Mech*., **40**(4), 1614-1622.

Gong, C.J., Wang, Y. Y., Peng, Y.C., Ding, W.Q., Lei, M. F., Da, Z. and Shi, C.H. (2022), "Three-dimensional coupled hydromechanical analysis of localized joint leakage in segmental tunnel linings", *Tunn. Undergr. Sp. Tech.*, **130**, 104726. https://doi.org/10.1016/j.tust.2022.104726.

Hassani, A.N., Katibeh, H. and Farhadian, H. (2016), "Numerical analysis of steady-state groundwater inflow into Tabriz line 2 metro tunnel, northwestern Iran, with special consideration of model dimensions", *Bull. Eng. Geol. Environ*., **75**(4), 1617-1627. https://doi.org/10.1007/s10064-015-0802-1.

Kabwe, E., Karakus, M. and Chanda, E.K. (2020), "Proposed solution for the ground reaction of non-circular tunnels in an elastic-perfectly plastic rock mass", *Comput. Geotech.*, **119**, 103354. https://doi.org/10.1016/j.compgeo.2019.103354.

Kim, N.Y., Park, D.H., Jung, H.S. and Kim, M.I. (2020), "Deformation characteristics of tunnel bottom after construction under geological conditions of long-term deformation", *Geomech. Eng*., **21**(2), 171-178. https://doi.org/10.12989/gae.2020.21.2.171.

Kolymbas, D. and Wagner, P. (2007), "Groundwater ingress to tunnels - The exact analytical solution", *Tunn. Undergr. Sp. Tech.*, **22**(1), 23-27. https://doi.org/10.1016/j.tust.2006.02.001.

Lei, S.Z. (1999), "An analytical solution for steady flow into a tunnel - Discussion - Reply", *Ground Water*, **37**(5), 643-644. https://doi.org/10.1111/j.1745-6584.1999.tb01154.x.

Liu, S., Zhao, S., Fu, D., Zhao, Q. and Zhu, Z. (2021), "Calculation of water and earth pressures on the top of shallow shield tunnels in marine and terrestrial sections under the condition of long-term water leakage", *Chinese J. Rock Mech. Eng.*, **40**(10), 2149-2160.

Lu, P., Chen, C., Liao, C. and Zhang, Y. (2019), "Model test on joint leakage in underwater shield tunnels", *Chinese J. Rock Mech. Eng.*, **38**(5), 993-1004.

Ming, H.F., Wang, M.S., Tan, Z.S. and Wang, X.Y. (2010), "Analytical solutions for steady seepage into an underwater circular tunnel", *Tunn. Undergr. Sp. Tech.*, **25**(4), 391-396. https://doi.org/10.1016/j.tust.2010.02.002.

Park, K.H., Owatsiriwong, A. and Lee, J.G. (2008), "Analytical solution for steady-state groundwater inflow into a drained circular tunnel in a semi-infinite aquifer: A revisit", *Tunn. Undergr. Sp. Tech.*, **23**(2), 206-209. https://doi.org/10.1016/j.tust.2007.02.004

Qiu, C., Zheng, Y., Zhang, Y., Tan, W. and Zhao, S. (2019),

"Discussion on classification method and criterion for the deep-buried and shallow-buried rock tunnels", *Modern Tunn. Technol*., **56**(1), 14-21.

Shin, J.H., Addenbrooke, T.I. and Potts, D.M. (2002), "A numerical study of the effect of groundwater movement on long-term tunnel behaviour", *Geotechnique*, **52**(6), 391-403. https://doi.org/10.1680/geot.52.6.391.38740.

Tang, Y., Chan, D.H. and Zhu, D.Z. (2018), "Analytical solution for steady-state groundwater inflow into a circular tunnel in anisotropic soils", *J. Eng. Mech.*, **144**(9), 06018003. https://doi.org/10.1061/(asce)em.1943-7889.0001502.

Wang, F. and Li, P.F. (2018), "An analytical model of seepage field for symmetrical underwater tunnels", *Symmetry-Basel*, **10**(7), 273. https://doi.org/10.3390/sym10070273.

Wang, Y.J., Yang, Y.Y., Su, F. and Wang, L.B. (2020), "Multiscale analytical method and its parametric study for lining joint leakage of shield tunnel", *Appl. Sci.-Basel*, **10**(23), 8528. https://doi.org/10.3390/app10238528.

Wei, G. and Lin, Y.F. (2013), "Monitoring and analysis of segment leakage of shield tunnels from Hangzhou subway system", *Disaster Advances*, **6**, 316-325.

Wongsaroj, J., Soga, K. and Mair, R.J. (2007), "Modelling of long-term ground response to tunnelling under St James's Park, London", *Geotechnique*, **57**(1), 75-90. https://doi.org/10.1680/geot.2007.57.1.75.

Wu, H.N., Shen, S.L., Chen, R.P. and Zhou, A. (2020), "Three-dimensional numerical modelling on localised leakage in segmental lining of shield tunnels", *Comput. Geotech.*, **122**, 103549. https://doi.org/10.1016/j.compgeo.2020.103549.

Yan, C.Z. and Zheng, H. (2017), "FDEM-flow3D: A 3D hydro-mechanical coupled model considering the pore seepage of rock matrix for simulating three-dimensional hydraulic fracturing", *Comput. Geotech.*, **81**, 212-228. https://doi.org/10.1016/j.compgeo.2016.08.014.

Zhang, D., Liu, Y. and Huang, H. (2013), "Leakage-induced settlement of ground and shield tunnel in soft clay", *J. Tongji University (Natural Science)*, **41**(8), 1185-1190, 1212. https://doi.org/10.3969/j.issn.0253-374x.2013.08.011.

Zhang, D.M., Xie, X.C., Zhou, M.L., Huang, Z.K. and Zhang, D.M. (2021), "An incident of water and soil gushing in a metro tunnel due to high water pressure in sandy silt", *Eng. Fail. Anal.*, **121**, 105196. https://doi.org/10.1016/j.engfailanal.2020.105196.

Zhang, F., Ji, W.X., Gao, Y.F., Leshchinsky, D. and Vahedifard, F. (2026), "Thermal effects on the stability of geosynthetic reinforced soil walls", *J. Geotech. Geoenviron. Eng.*, **152**(1). https://doi.org/10.1061/JGGEFK.GTENG-14248.

Zhang, J., Li, S.C., Li, L.P., Zhang, Q.Q., Xu, Z.H., Wu, J. and He, P. (2017), "Grouting effects evaluation of water-rich faults and its engineering application in Qingdao Jiaozhou Bay Subsea Tunnel, China", *Geomech. Eng.*, **12**(1), 35-52. https://doi.org/10.12989/gae.2017.12.1.035.

Zhang, S.L., Cheng, X.S., Zhou, X.H. and Sun, Y. (2023), "Face stability analysis of large-diameter underwater shield tunnel in soft-hard uneven strata under fluid-solid coupling", *Geomech. Eng.*, **32**(2), 145-157. https://doi.org/10.12989/gae.2023.32.2.145.